International Journal of Heat and Mass Transfer 113 (2017) 210–216

Contents lists available at ScienceDirect

International Journal of Heat and Mass Transfer

journal homepage: www.elsevier.com/locate/ijhmt

Supersonically sprayed, triangular copper lines for pool boiling enhancement

Hong Seok Jo [a,1], Jong-Gun Lee [a,1], Seongpil An [a], Tae Gun Kim [a], Scott C. James [b], Jeehoon Choi [c,*], Sam S. Yoon [a,*]

[a] School of Mechanical Engineering, Korea University, Seoul 02841, Republic of Korea
[b] Depts. of Geosciences and Mech. Eng., Baylor University, Waco, TX 76798, USA
[c] LG Electronics Inc., Seoul, Republic of Korea

ARTICLE INFO

Article history:
Received 10 April 2017
Received in revised form 17 May 2017
Accepted 17 May 2017

Keywords:
Supersonic spraying
Copper nanoparticles
Pool boiling
Superheat temperature
Critical heat flux

ABSTRACT

Pool boiling is a mechanism by which heat is removed through nucleation of bubbles at the heated surface. Because of the ever-increasing demand for miniaturization of more powerful electronic devices, heat flux requirements grow. Herein, we introduce a rapid, scalable supersonic spray-coating technique that produces micro-scale lines with triangular cross sections. The surface of each triangular line is textured and provides numerous nucleation sites. Pathways of escaping bubbles experience minimal interference because of the triangular shape of the lines. These rising bubbles remove heat efficiently and facilitate rapid cooling. Both critical heat flux and the effective heat transfer coefficient increased significantly under the optimal coating condition, which is identified. The effect of the number of the patterned lines was studied. The coolant contact angle against the lined surface was investigated to quantify wettability and capillary effects. Bubble formation was visualized with a CCD camera and the triangular-shaped lines were characterized by scanning electron microscopy and an optical profiler.

1. Introduction

Over the last decade, the number of internet mobile devices such as smart phones, and tablet PCs has increased exponentially. Nano-scale integrated circuit chips and high-capacity compact batteries have made it possible for these devices not only to provide entertainment, information, and location-based services for personal use, but also to store and manipulate large data sets. However, both of these features are hindered by necessarily increasing heat fluxes and it is expected that classical cooling solutions will not be able to satisfy future thermal demands [1,2]. Enhanced and manufacturing-friendly cooling technologies are subject to the limitations imposed by small overall volumes, light-weight design, and effective cooling performance.

Micro-scale, phase-change, heat-transfer systems such as micro heat pipes and vapor chambers, which are easy to control with no external pumping requirements, are viewed as two of the best potential solutions to thermal-management problems [3–9]. These systems use capillary forces from grooves machined into a wick-like surface. The working fluid evaporates at hot spots and is condensed back to liquid in a cooler region. The pathways of the phase changing liquid are provided by grooved structures that increase capillary forces.

At increased heat fluxes, excessive bubble growth may occur locally, preventing efficient cooling by evaporation. In addition, local dry-spot formation can obstruct pathways of circulating liquid supply during bubble formation. Grooved surfaces have been used to counter these problems through local curvature that increases capillary forces to draw in liquid more efficiently.

The grooves can be constructed by chemical etching, vapor deposition, or skiving during metallic manufacturing, which involves multiple manufacturing steps and therefore inhibit cost competitiveness.

For this reason, we introduce a new technique for constructing grooves in our case (lines) by supersonic spraying, which is rapid, scalable, and commercially viable. Metal particles are entrained into a supersonic stream by expanding pressurized air at high temperatures [10]. By converting the thermal and pressure energy into kinetic energy, a supersonic stream is generated. The accelerated metal particles adhere onto the substrate after passing through a patterned mask. Ultimately, lines with a triangular cross-sectional shape are generated [11].

* Corresponding authors.
E-mail addresses: choijeehoon@gmail.com (J. Choi), skyoon@korea.ac.kr (S.S. Yoon).
[1] These authors have equally contributed.

http://dx.doi.org/10.1016/j.ijheatmasstransfer.2017.05.070
0017-9310/

Excessive nano-texturing can interfere with the pathways of rising bubbles. A thick nanotextured layer can trap nucleated bubbles leading to increased thermal resistance and hindered pool boiling performance. Our triangular shape facilitates rapid detachment of nucleating bubbles with minimal interference against the rising bubbles (imagine how nucleated bubbles would be trapped if the shape was an upside-down triangle). Bubble coalescence is minimized because of their rapid detachment from the grooves. Therefore, issues of dry out and pathway obstruction are minimized. Ample supply of liquid and continuous wetting are facilitated. These nano-porous lines also result in numerous bubble nucleation sites. The triangular-shaped lines stimulate bubble generation through increased capillary forces allowing for uniform wetting along the line while increasing the area for bubble nucleation.

We have previously shown how nano-scale structures textured on flat surfaces have significant potential for application to miniature electronics cooling devices because wettability, critical heat flux (CHF), and effective heat transfer coefficients (h_{eff}) are notably improved [12,13]. Herein, we expect that increasing the number of lines will increase the CHF and h_{eff} through more nucleation sites and by increasing the surface area. However, too many closely spaced lines can lead to bubble coalescence and film boiling, which would decrease heat transfer.

2. Experimental setup

2.1. Materials

Copper powder (LeesChem Co., Korea) with an average size of 1 μm was used to coat a copper substrate [11]. HFE-7100 (NovecTM Engineering Fluid, 3 M), which is non-ozone-depleting fluid with low toxicity, was used as the coolant in this study. This coolant has a high latent heat of vaporization allowing for enhanced nucleate boiling and CHF. Table 1 lists the physical properties of HFE-7100 [14].

2.2. Supersonic spray coating

The supersonic cold spray setup consisting of a compressor, powder feeder (Praxair 1264i, USA), nozzle, and an *x-y* stage (Fig. 1) was used to pattern the substrate with multiple triangular-cross-section copper lines. The compressor operated at $P_0 = 6$ bar and the gas temperature was $T_0 = 320$°C to add thermal energy to the accelerating air, which converted to kinetic energy yielding a supersonic air stream. The nozzle-to-substrate distance was 55 mm and the size of the masks used to produce the patterned lines was $50 \times 50\ mm^2$. The steel masks have variable-spaced rectangular slits to pattern the lines. The powder feeder supplied Cu particles at 25 L/min and the particles were coated onto the substrate along the length of mask as the nozzle travels at 35 mm/s for a total of two passes. The number of Cu lines (N_{line}) was developed as shown in Fig. 2a.

2.3. Pool boiling experimental setup

Pool boiling tests were carried out using the experimental setup shown in Fig. 3. Part 1 (Fig. 3a) of the test section consists of a test sample, three thermocouples, an aluminum rod for transferring heat from heaters to the sample, four heaters, and a Teflon case. Part 2 (Fig. 3b) of the boiling experiment includes a condenser, three preheaters, a thermocouple, a test chamber, and a Teflon cap.

Four cylindrical cartridge heaters in an aluminum rod ($k_{Al} = 210\ W\ m^{-1}\ K^{-1}$) were connected to the power supply (Slidac, 1 KVA, Dae Kwang Electric Co) and three K-type thermocouples (Omega Inc. with accuracies of ±0.3°C, thickness = 1 mm) were placed along the rod at regular intervals of 8 mm to measure three different temperature (T_1, T_2, and T_3). By encapsulating the rod in a Teflon case and cap ($k = 0.25\ W\ m^{-1}\ K^{-1}$), heat losses were minimized. The sample was fixed using a thermal grease (DOW CORNING, TC-5026, $k_g = 2.89\ W\ m^{-1}\ K^{-1}$) to reduce contact thermal resistance between the sample and the aluminum rod.

Table 1
Physical properties of the HFE-7100 Engineering fluid.

Physical properties	HFE-7100 (0.1 MPa)
Boiling point (°C)	61
Density of liquid ($kg\ m^{-3}$)	1370.2
Density of vapor ($kg\ m^{-3}$)	987
Viscosity of liquid ($kg\ m^{-1}\ s^{-1}$)	3.70×10^{-4}
Surface tension of liquid-vapor interface ($N\ m^{-1}$)	1.019×10^{-2}
Specific heat of liquid ($J\ kg^{-1}\ K^{-1}$)	1255
Enthalpy of vaporization ($J\ kg^{-1}$)	111.6

The test chamber was held between top and bottom aluminum plates and three preheaters were submerged in the coolant. To maintain the saturated temperature of the coolant, the preheaters were supplied 30 V by the power supply (Slidac, 0.5 KVA, Dae Kwang Electric Co). The condensing unit, a spiral tube circulating cooling water at 5°C from the chiller (AP15R-30-V11B, VWR Ad), was connected to the top aluminum plate to maintain coolant levels.

Prior to the experiments, the temperatures of the coolant and sample were stabilized by applying 60 V to the four cartridge heaters for 30 min and pool boiling tests started when the coolant temperature varied no more than ±0.1°C. Voltage was stepped at 5 V every 10 min so that the temperatures of three thermocouples reached steady state. Voltage steps continued until pool boiling was achieved and the substrates reached CHF, which was identified as the last steady-state heat value before temperatures rose sharply.

2.4. Characterization

Cross-sectional and plan views of a Cu line were measured by a field-emission scanning electron microscope (FE-SEM, S-5000, Hitachi) at 15 kV. Roughness and 3D images were characterized by an optical profiler (Veeco, NT-1100). Capillary phenomena were measured by dipping the sample into a coolant and taking snapshots with a high-speed camera (Phantom 9.1, Vision research Inc.). Coolant contact angles were analyzed using an image-capture and measurement solution (I'MEASER 3.0, ING. PLUS).

3. Results and discussion

3.1. Triangular copper lines

Fig. 2b shows the morphology of the line. As in the previous study [11], Cu particles were sprayed uniformly through the nozzle, but preferentially deposited in the center because of recirculation zones forming at each edge of the mask. As a result, Cu particles were deposited in a triangular shape as shown in Fig. 2b. In addition, the height of the triangle increased as the number of coating passes increased [11]. For this study, the number of spray passes was fixed at 2 and the height (h) and width (w) of the triangular Cu line were 128 and 348 μm, respectively, and thus their aspect ratio was $\gamma = h/w = 0.37$. In conjunction with the SEM images, 3D images from an optical profiler were acquired as shown in Fig. 2c, which shows the patterned lines for various spacing (λ). The h of these triangles was constant for all three cases.

At $\Delta T_{sat} = 13$°C (Fig. 4a), bubble sizes were fairly uniform across the three cases and there was only a slight difference in the num-

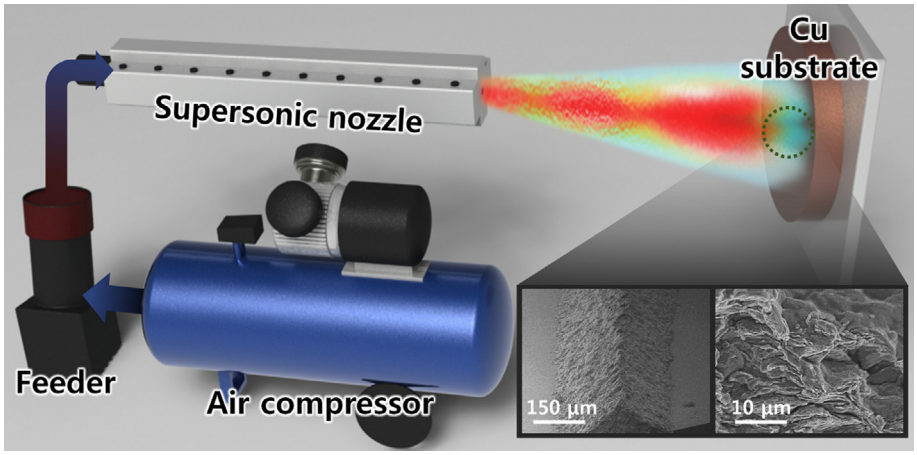

Fig. 1. Schematic of the copper particle coating process on a copper substrate.

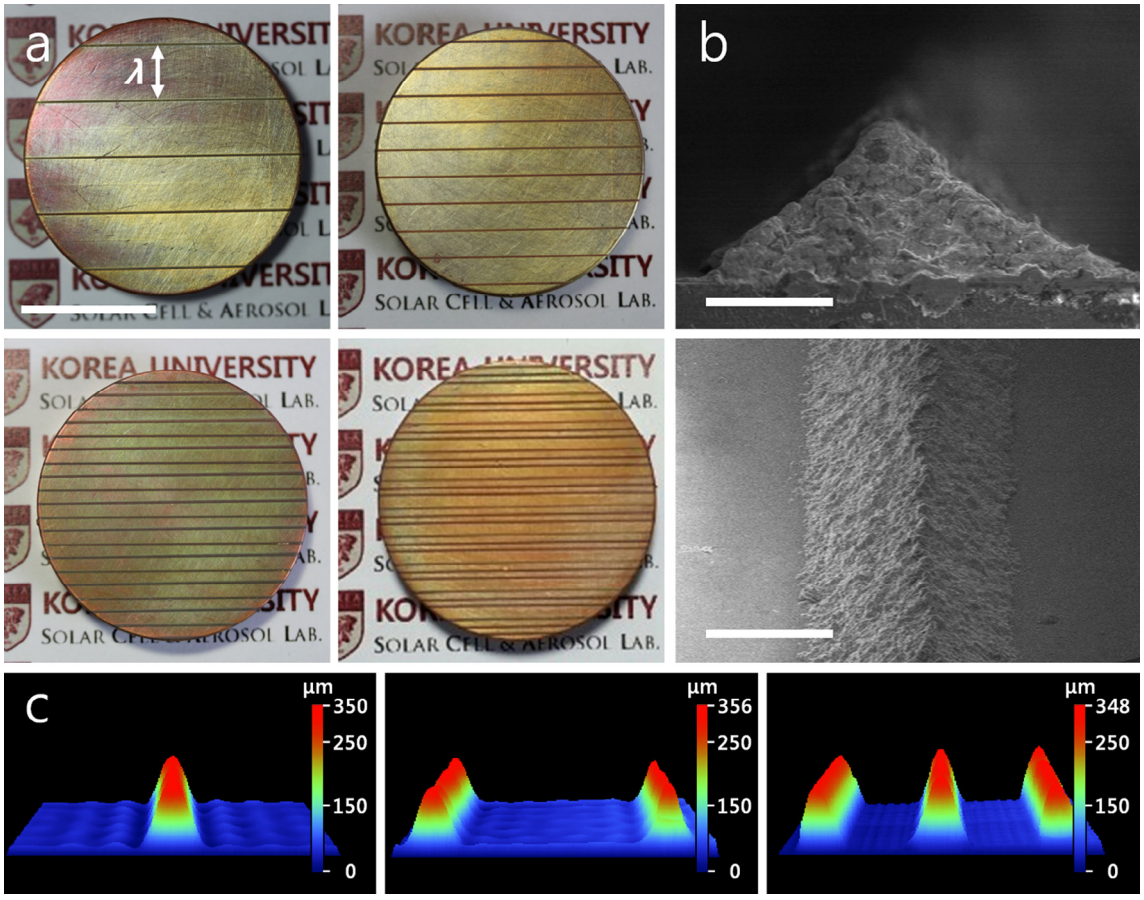

Fig. 2. (a) Photographs for N_{line} from 5 to 30 (the scale bar is 25 mm), (b) Plan-view and cross-sectional SEM images of the triangular line structure (the scale bars in the top and bottom figures are 100 and 200 μm, respectively), and (c) optical profiler for N_{line} = 10, 20, and 30 from left to right.

ber of generated bubbles for N_{line} = 5, 20, and 30. Compared to ΔT_{sat} = 13°C, at ΔT_{sat} = 25°C (Fig. 4b), bubbles were smaller with the most number of bubbles per line at N_{line} = 20. For N_{line} = 20 and 30, bubbles were similarly sized, but larger for N_{line} = 5.

3.2. Pool boiling heat-transfer validation

Heat flux was estimated using Fourier's Law (one-dimensional, steady state):

$$q_t'' = k_{A1}\frac{T_2 - T_1}{\Delta x_{12}} = k_{A1}\frac{T_3 - T_2}{\Delta x_{23}}. \quad (1)$$

Temperatures T_1, T_2, and T_3 in Fig. 3a differed according to conduction across Δx_{12} and Δx_{23}, which are both equal to the 8 mm between thermocouples along the aluminum rod (k_{Al} = 210 W m^{-1} K^{-1}). The surface temperature of the sample (T_w) was difficult to measure directly, therefore, T_w was derived using Eq. (1) and q_t''= $(T_1 - T_w)/(\Delta x_g/k_g + \Delta x_w/k_{Cu})$, which is the heat flux through the thermal grease layer to the surface of the substrate:

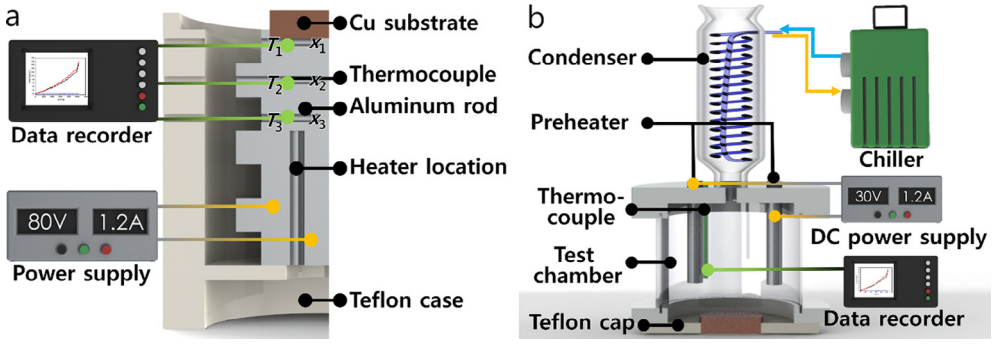

Fig. 3. Experimental setup: (a) Part 1: test section and (b) Part 2: boiling-experiment section.

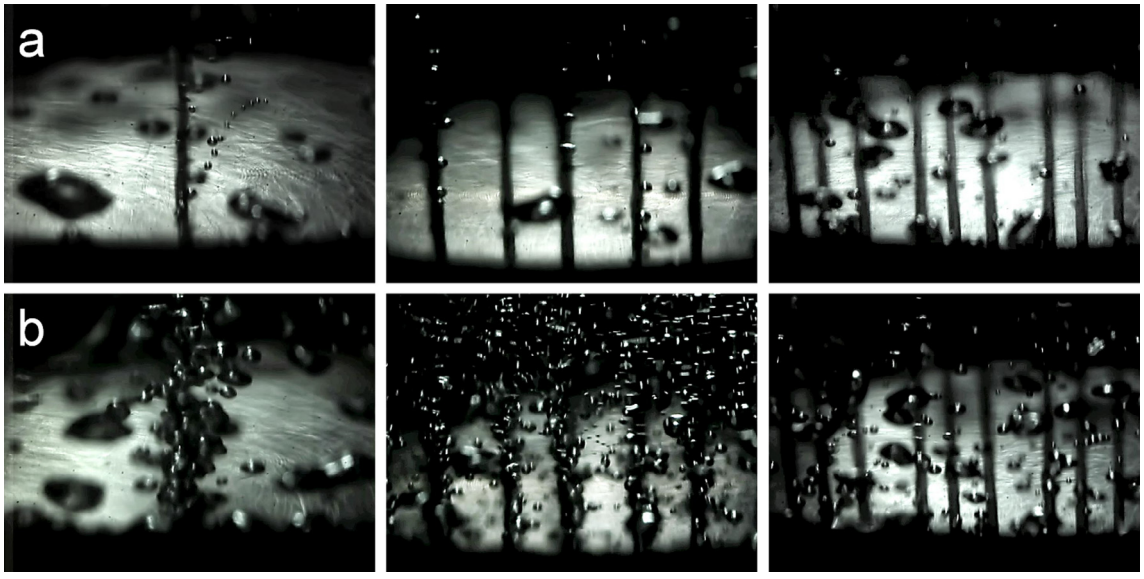

Fig. 4. Snapshots of pool boiling with the triangular lines as a function N_{line} = 5, 20, and 30 at ΔT_{sat} = (a) 13 and (b) 25°C.

$$T_w = T_1 - k_{Al}\frac{(T_2 - T_1)}{\Delta x_{12}}\left(\frac{\Delta x_g}{k_g} + \frac{\Delta x_w}{k_{Cu}}\right), \quad (2)$$

where k_{Cu} = 401 W m^{-1} K^{-1}) is the thermal conductivity of the copper substrate, Δx_g and Δx_w are the thickness of the thermal grease layer and the distance between thermocouple T_1 and the surface of the substrate, respectively. Δx_g was specified as the averaged thickness of the thermal grease measured 10 times using an electronic vernier caliper (BDJK-565, resolution = 0.005 mm, limit error = ±0.015 mm). Error was 7% across the 10 measurements of thermal grease thickness. In Eq. (2), the superheat (ΔT_{sat}) is ΔT_{sat} = $T_w - T_f$, where T_f is the saturated temperature of the coolant.

Finally, h_{eff} was estimated using Newton's Law of Cooling as:

$$h_{eff} = \frac{q''_t}{\Delta T_{sat}}. \quad (3)$$

In addition, our experimental results were compared to the modified Rohsenow equation in Fig. 5a, which is only strictly applicable to a perfectly smooth surface [15]:

$$q''_t = C_r \mu_l h_v \left[\frac{g(\rho_l - \rho_v)}{\sigma}\right]^{1/2}\left(\frac{c_p \Delta T_{sat}}{C_{s,f} h_v Pr_l^n}\right)^3, \quad (4)$$

where subscripts $(\,)_l$ and $(\,)_v$ are liquid and vapor states, μ and h_v are a viscosity of the liquid and an enthalpy of vaporization, respectively. g, ρ, and σ are gravitational acceleration, density, and surface tension of the liquid, respectively, and c_p and Pr are a specific heat of liquid and the Prandtl number, respectively [16]. The constant, C_r, varies with N_{line} except for the uncoated substrate where C_r = 1 and data were matched by adjusting $C_{s,f}$ = 0.76 using n = 1.7 for the coolant.

Using an error propagation technique [17], the uncertainty in our experimental heat flux estimate was:

$$U_q = \sqrt{\left(\frac{\partial q}{\partial V}U_V\right)^2 + \left(\frac{\partial q}{\partial I}U_I\right)^2 + \left(\frac{\partial q}{\partial A}U_A\right)^2}. \quad (5)$$

The aluminum rod was covered with a Teflon case to reduce heat loss, nevertheless, a heat loss of about 1% was incurred. The uncertainty in our study is ±4.3% for q''_t from Eq. (5).

3.3. Effects of N_{line} on CHF and h_{eff}

Fig. 5a and b relate q''_t to ΔT_{sat} on uncoated and the line-patterned surfaces for $5 \le N_{line} \le 30$. The boiling curves indicate that both the boiling heat transfer and CHF were enhanced by the textured surfaces compared to the untreated surface. As shown in Fig. 5a, the onset of boiling appears earlier as N_{line} increases up to 20. The roughness increased with increasing N_{line} as indicated in Table 2.

In Fig. 5b and c, both CHF and h_{eff} increased with increasing N_{line} up to 20, beyond which performance not ably decreased. The CHF reached a maximum value of 168 kW m^{-2} at N_{line} = 20. ΔT_{sat} was

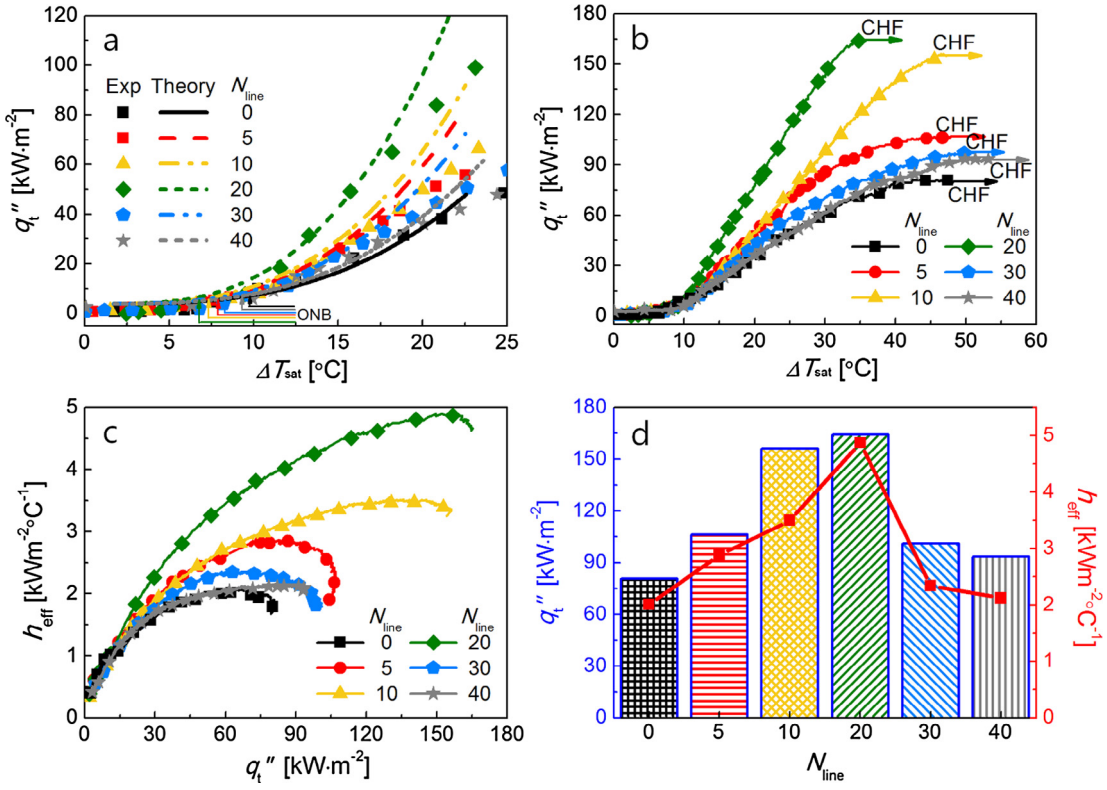

Fig. 5. (a) Comparison between the experimental and theoretical q_t'', (b) q_t'' versus ΔT_{sat} for N_{line} from 0 to 40. (c) h_{eff} versus q_t'' for N_{line} from 0 to 40. (d) CHF and h_{eff} as a function of N_{line}.

also lowest for $N_{line} = 20$ indicating that the temperature at the heated surface (T_s) was the lowest as $\Delta T_{sat} = T_s - T_\infty$ where T_∞ was fixed at 60.5°C. For $N_{line} = 30$, CHF decreased to 92 kW m^{-2}, which is lower than for $N_{line} = 5$ (98 kW m^{-2}). Too many lines decreases wettability and thus heat transfer was hindered by hydrophobic behavior, which will be explained in detail later. All coated substrates ($N_{line} = 5$–40) demonstrated improved cooling performance over an untreated substrate. This trend is also true for h_{eff} as shown in Fig. 5c. Here, the highest h_{eff} was observed at $N_{line} = 20$, which indicates that this is the optimal number of lines for both CHF and h_{eff}. Fig. 5d compares the CHF and h_{eff} across all cases.

The effective heat transfer coefficient, h_{eff}, is a strong function of N_{line} although it comprises both uncoated and lined surfaces: $h_{eff} = h_{eff\_u} + h_{eff\_l}$. The contribution of each can be quantified using a one-dimensional model [15]. The total heat flux for an area of 20×20 mm^2 at $\Delta T_{sat} = 30$°C is:

$$q_t'' = q_u'' + q_l'' = h_{eff\_u}\Delta T_{sat} + h_{eff\_l}\Delta T_{sat}\,, \tag{6}$$

where subscripts $()_u$ and $()_l$ are the uncoated and lined surfaces, respectively. In addition, by applying the distributive law to h_{eff_u}, and ΔT_{sat}, the expression is

$$q_t'' = h_{eff\_u}\Delta T_{sat}\left(\frac{h_{eff\_l}}{h_{eff\_u}} + 1\right) = C_h \cdot h_{eff\_u}\Delta T_{sat}, \tag{7}$$

where $C_h = h_{eff\_l}/h_{eff\_u} + 1$ is a calibration constant between the heat flux of lined and uncoated surfaces. C_h was calculated using the experimental results in Table 2 and the comparison with h_{eff} for the lined and uncoated surfaces was obtained. The ratio (h_{eff_l}/h_{eff_u}) is compared to q_t'', which varies with N_{line}. As in Fig. 6a, these ratios are less than one, except for $N_{line} = 20$ where $h_{eff\_l}/h_{eff\_u} = 1.35$. It should be noted that all other cases ($N_{line} = 5$, 10, 30 and 40) show that the triangular lines increase h_{eff} through additional h_{eff_l}. However, the h_{eff_l} increase was never greater than the uncoated heat transfer coefficient, h_{eff_u}, except for $N_{line} = 20$. The copper lines have increased the surface wettability up to $N_{line} = 20$. However, pool boiling performance degrades for $N_{line} > 20$ because surface wettability decreases.

Fig. 6b shows the ratio of the h_{eff_l}/h_{eff_u} normalized by N_{line} indicating the heat transfer capacity per copper line. This type of analysis is useful when assessing how many lines to use to maximize efficiency. In commercial applications, a compromise is often made to reduce production costs. For example, $N_{line} = 20$ may yield the best CHF and h_{eff}; however, if $N_{line} = 10$ has comparable CHF and h_{eff}, this may be more desirable in terms of manufacturing. This kind of judgement can be made based on the results shown in Fig. 6b. $N_{line} > 20$ is least desirable because of low $h_{eff\_l}/(N_{line} \cdot h_{eff\_u})$. On the other hand, all other cases ($N_{line} = 5$, 10, and 20) show comparable efficiency; each line is responsible for a nearly equal amount of heat transfer up to $N_{line} = 20$. Therefore, if maximum heat needs to be transferred, $N_{line} = 20$ should be implemented.

3.4. Effects of N_{line} on wettability

Increasing N_{line} provides more nucleation sites for increased bubble generation because of the surface area increase. In addition, the unique triangular structure of the lines helps bubbles to be released more efficiently due to decreased interference. However, these favorable phenomena are effective only up to a certain N_{line} because of changes to wettability (increased hydrophobicity).

We have measured the effects of N_{line} on CHF and h_{eff}. The number of lines increases both CHF and h_{eff} up to $N_{line} = 20$, beyond which pool boiling performance degrades. The coolant contact angle is also responsible for this transition between $N_{line} = 20$ and 30. As seen in Fig. 6c, the coolant contact angle decreases until $N_{line} = 20$ whereupon it increases. In addition, when $N_{line} = 30$, bub-

Table 2
Interspace distance, roughness, constants, and contact angle for different N_{line}.

N_{line}	λ (mm)	Roughness (μm)	C_r	C_h	θ [°]
5	8	–	1.4	1.4	26
10	4	4.8	1.5	1.7	23
20	2	9.3	2.4	2.3	11
30	1.3	18.1	1.2	1.2	25
40	1	21.0	1.1	1.1	28

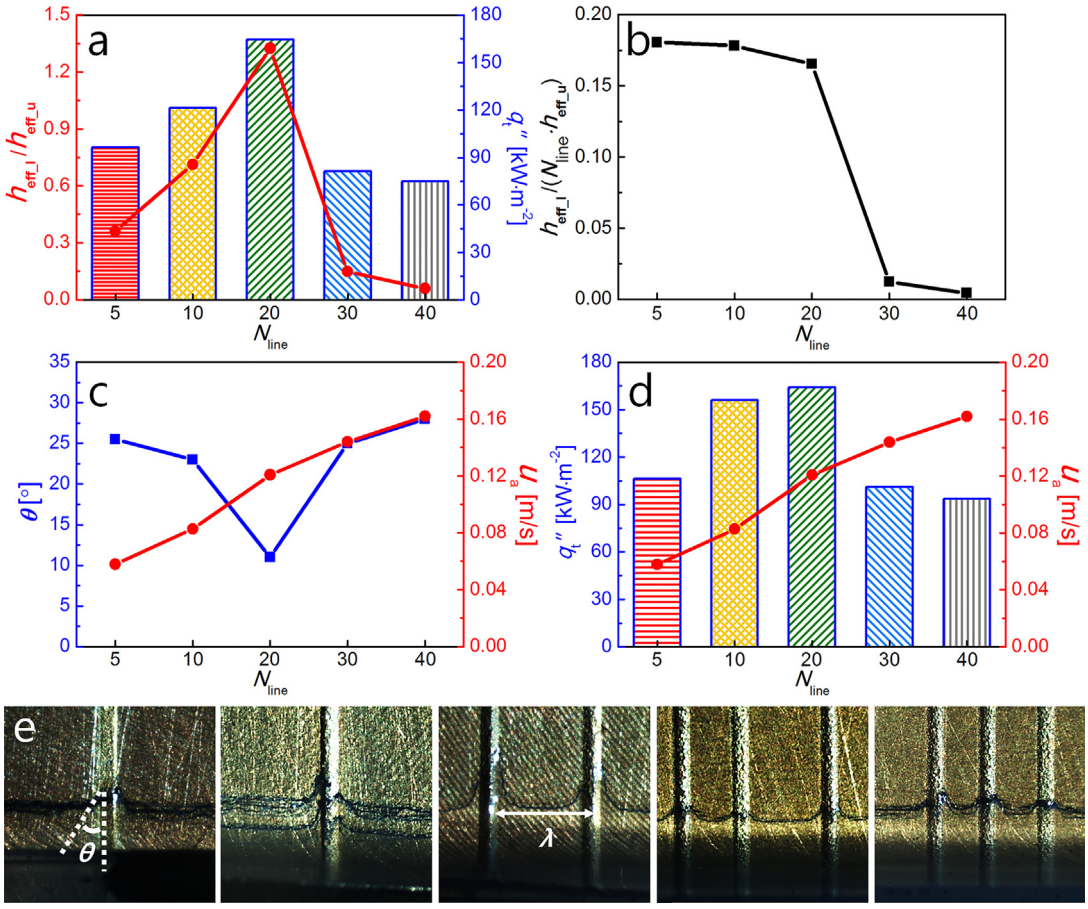

Fig. 6. For N_{line} from 5 to 40 for (a) h_{eff}, (b) the single-line normalized h_{eff} ratios, (c) comparisons of θ and u_a, (d) CHF and u_a, and (e) θ of the coolant due to capillary effects.

bles coalesce causes film boiling, which degrades pool-boiling performance.

Another important factor that affects the overall pool boiling performance is the roughness of the textured surface. Electronics applications need to be continuously cooled by rewetting hot spots [18,19]. For example, in a heat pipe system, rising vapor condenses along the inside wall of the pipe. Heat transfer generally increases when the wall surface is grooved (roughened). Therefore, the more grooves, the greater the heat transfer. Wettability was quantified by the coolant contact angle shown in Fig. 6e.

The wicking velocity is important for its role in providing coolant, the degree to which is determined by the surface permeability and capillarity. Permeability governs the wicking velocity, which affects pool boiling performance. For example, it is desirable that the heated surface be continuously and rapidly supplied with liquid coolant. If the heated surface is appropriately textured to increase the flow rate, bubbles are efficiently nucleated and released for continuous pool boiling. If the permeability is too low, then rapid heating will lead to large bubble formation through coalescence, which leads to system failure due to dry-out.

In Fig. 6c, the roughness of the lined surface is characterized by the coolant velocity, u_a. When N_{line} increases, surface roughness increases. According to [18], inflow rate can be evaluated through the relationship between capillary pressure and the Darcy friction pressure drop. However, the effect of the Darcy friction pressure drop is imperceptible in our study because the length scale of λ is much larger than the bubble diameter. Therefore, the inflow rate was derived using the Darcy-Weisbach equation and the capillary pressure [18,20]:

$$\frac{2\sigma\cos\theta}{\lambda} = \frac{1}{2}\rho u_a^2, \tag{8}$$

where σ, θ, and ρ are the surface tension, the contact angle, and the density of the coolant, respectively. The right-hand term for capillary pressure is a function of λ and θ [21–23]. Coolant velocity is estimated from Eq. (8) as:

$$u_a = \sqrt{\frac{4\sigma\cos\theta}{\rho\lambda}}. \tag{9}$$

u_a depends on the geometric properties of θ and λ. As shown in Fig. 6e, θ changes with λ. Fig. 6c shows how θ and u_a vary with λ (see Table 2). Although λ is inversely proportional to N_{line}, θ has a minimum of 10° at $\lambda = 2$ mm, which corresponds to $N_{line} = 20$. On the other hand, u_a increases with decreasing λ (or increasing N_{line}) according to Eq. (9), as shown in Fig. 6c. The influence of λ on u_a is more pronounced than that of $\cos\theta$, which also varies with N_{line} as shown in Fig. 6c. Upon decreasing λ from 8 to 1 mm (which corresponds to N_{line} from 5 to 40), u_a increased from 0.06 to 0.16 m/s indicating improved liquid mobility. However, this trend does not explain the reversing trend for CHF and h_{eff} at $N_{line} = 20$ evident in Fig. 5. Instead, changing wettability from Fig. 6c explains the decrease in CHF and h_{eff} seen in Fig. 5 for $N_{line} = 30$. This suggests that wettability is the dominant factor in CHF and h_{eff} for this line spacing while the latter is also an important factor for rapid flow of coolant.

4. Conclusion

Copper nanoparticles were deposited as lines with a triangular cross section using supersonic cold spraying. The triangular shape facilitated bubble release without interference and enhanced CHF and h_{eff} for all cases. Of the tested cases, $N_{line} = 20$ yielded the highest CHF and h_{eff} because of its high contact angle that allowed the closest contact between the cooling liquid and the heated surface. It should be noted that too many lines adversely impacts CHF and h_{eff} and thus an optimal fabrication condition must be identified. In addition, too many closely spaced lines can lead to bubble coalescence and film boiling, which lead to system failure due to dry-out. The supersonic spray-coating technique used herein is rapid, scalable, and is easily adaptable to a roll-to-roll process, which has potential for commercial manufacturing of cost-effective pool boiling devices.

Acknowledgement

This research was supported by the Technology Development Program to Solve Climate Changes of the National Research Foundation (NRF) funded by the Ministry of Science, ICT & Future Planning (2016M1A2A2936760), NRF-2017R1A2B4005639, and GFHIM of NRF-2013M3A6B1078879. This work (C0421241) was also supported by Business for Cooperative R&D between Industry, Academy, and Research Institute funded Korea Small and Medium Business Administration.

References

[1] A. Bejan, G. Tsatsaronis, Thermal Design and Optimization, John Wiley & Sons, 1996.
[2] D.S. Steinberg, Cooling techniques for electronic equipment, Wiley-Interscience, New York, 1980, 387 p.
[3] L. Vasiliev, Micro and miniature heat pipes–Electronic component coolers, Appl. Therm. Eng. 28 (4) (2008) 266–273.
[4] S. Lips, F. Lefèvre, J. Bonjour, Nucleate boiling in a flat grooved heat pipe, Int. J. Therm. Sci. 48 (7) (2009) 1273–1278.
[5] S.-C. Wong, C.-W. Chen, Visualization and evaporator resistance measurement for a groove-wicked flat-plate heat pipe, Int. J. Heat Mass Transf. 55 (9) (2012) 2229–2234.
[6] X. Li, J. Wang, Q. Hu, L. Bao, H. Zhang, Experimental and theoretical research on capillary limit of micro heat pipe with compound structure of sintered wick on trapezium-grooved substrate, Heat Mass Transf. 49 (3) (2013) 381–389.
[7] Y.S. Ju, M. Kaviany, Y. Nam, S. Sharratt, G. Hwang, I. Catton, E. Fleming, P. Dussinger, Planar vapor chamber with hybrid evaporator wicks for the thermal management of high-heat-flux and high-power optoelectronic devices, Int. J. Heat Mass Transf. 60 (2013) 163–169.
[8] Y. Luo, G. Liu, L. Zou, Y. Yang, X. Wang, Experimental investigation of microheat pipes for high-power light-emitting diode modules, Micro Nano Lett. 8 (10) (2013) 646–649.
[9] B. He, M. Wei, S. Somasundaram, C.S. Tan, E.N. Wang, Experiments on the ultrathin silicon vapor chamber for enhanced heat transfer performance, in: Thermal and Thermomechanical Phenomena in Electronic Systems (ITherm), 2016 15th IEEE Intersociety Conference on, IEEE, 2016, pp. 569–573.
[10] J.-G. Lee, D.-Y. Kim, B. Kang, D. Kim, S.S. Al-Deyab, S.C. James, S.S. Yoon, Thin film metallization by supersonic spraying of copper and nickel nanoparticles on a silicon substrate, Comput. Mater. Sci. 108 (2015) 114–120.
[11] D.-Y. Kim, J.-J. Park, J.-G. Lee, D. Kim, S.J. Tark, S. Ahn, J.H. Yun, J. Gwak, K.H. Yoon, S. Chandra, Cold spray deposition of copper electrodes on silicon and glass substrates, J. Therm. Spray Technol. 22 (7) (2013) 1092–1102.
[12] S. An, D.-Y. Kim, J.-G. Lee, H.S. Jo, M.-W. Kim, S.S. Al-Deyab, J. Choi, S.S. Yoon, Supersonically sprayed reduced graphene oxide film to enhance critical heat flux in pool boiling, Int. J. Heat Mass Transf. 98 (2016) 124–130.
[13] H.S. Jo, S. An, H.G. Park, M.-W. Kim, S.S. Al-Deyab, S.C. James, J. Choi, S.S. Yoon, Enhancement of critical heat flux and superheat through controlled wettability of cuprous-oxide fractal-like nanotextured surfaces in pool boiling, Int. J. Heat Mass Transf. 107 (2017) 105–111.
[14] M.S. El-Genk, H. Bostanci, Saturation boiling of HFE-7100 from a copper surface, simulating a microelectronic chip, Int. J. Heat Mass Transf. 46 (10) (2003) 1841–1854.
[15] T.L. Bergman, F.P. Incropera, D.P. DeWitt, A.S. Lavine, Fundamentals of Heat and Mass Transfer, John Wiley & Sons, 2011.
[16] L.-T. Chen, Heat transfer to pool-boiling Freon from inclined heating plate, Lett. Heat Mass Trans. 5 (2) (1978) 111–120.
[17] J. Holman, Analysis of experimental data, Exp. Methods Eng. (2001) 48–143.
[18] S.H. Kim, G.C. Lee, J.Y. Kang, K. Moriyama, M.H. Kim, H.S. Park, Boiling heat transfer and critical heat flux evaluation of the pool boiling on micro structured surface, Int. J. Heat Mass Transf. 91 (2015) 1140–1147.
[19] P. Carman, Fluid flow through granular beds, Chem. Eng. Res. Des. 75 (1997) S32–S48.
[20] G. Brown, The Darcy-Weisbach Equation, Oklahoma State University-Stillwater, 2000.
[21] J. Eick, R. Good, A. Neumann, Thermodynamics of contact angles. II. Rough solid surfaces, J. Colloid Interface Sci. 53 (2) (1975) 235–248.
[22] F. Ferrero, Wettability measurements on plasma treated synthetic fabrics by capillary rise method, Polym. Testing 22 (5) (2003) 571–578.
[23] G. Bracco, B. Holst, Surface science techniques, Springer Science & Business Media, 2013.